Three-dimensional high spatial localization of efficient resonant energy transfer from laser-assisted precipitated silver clusters to trivalent Europium ions

Yannick Petit, Gustavo Galleani, Guillaume Raffy, Jean-Charles Desmoulin, Veronique Jubera, André del Guerzo, Andrea Simone Stucchi de Camargo, Lionel Canioni, Thierry Cardinal

▶ **To cite this version:**

Yannick Petit, Gustavo Galleani, Guillaume Raffy, Jean-Charles Desmoulin, Veronique Jubera, et al.. Three-dimensional high spatial localization of efficient resonant energy transfer from laser-assisted precipitated silver clusters to trivalent Europium ions. Crystals, 2021, 11 (2), pp.148. 10.3390/cryst11020148 . hal-03130650

HAL Id: hal-03130650
https://hal.science/hal-03130650

Submitted on 3 Feb 2021

HAL is a multi-disciplinary open access archive for the deposit and dissemination of scientific research documents, whether they are published or not. The documents may come from teaching and research institutions in France or abroad, or from public or private research centers.

L'archive ouverte pluridisciplinaire **HAL**, est destinée au dépôt et à la diffusion de documents scientifiques de niveau recherche, publiés ou non, émanant des établissements d'enseignement et de recherche français ou étrangers, des laboratoires publics ou privés.

Three-dimensional high spatial localization of efficient resonant energy transfer from laser-assisted precipitated silver clusters to trivalent Europium ions

Y. Petit,[1,2,*] G. Galleani,[1,3] G. Raffy[4], J.C. Desmoulin[1], V. Jubera[1], A. Del Guerzo[4], A. Camargo[3], L. Canioni[2], T. Cardinal[1]

[1] *Univ. Bordeaux, CNRS, ICMCB, UPR 9048, F-33608 Pessac, France*

[2] *Univ. Bordeaux, CNRS, CEA, CELIA, UMR 5798, F-33400 Talence, France*

[3] *Institute of Physics, USP, CP369, 13560-970, Sao Carlos, SP, Brazil*

[4] *Univ. Bordeaux, CNRS, ISM, UMR 5255, F-33400 Talence, France*

**Corresponding author: yannick.petit@u-bordeaux.fr*

ABSTRACT

We report on the 3D precipitation, using a direct laser writing approach, of highly fluorescent silver clusters in a Eu^{3+}-doped silver-containing zinc phosphate glass. Micro-spectroscopy of fluorescence emission shows the ability to continuously adjust the local tri-chromatic coordinates in the CIE chromaticity diagram between red and white colors, thanks to the laser-deposited dose and resulting tunable combination of emissions from Eu^{3+} and silver clusters. Moreover, CW and time-resolved FAST-FLIM spectroscopies showed a significant enhancement of the fluorescence emission of Eu^{3+} ions while being co-located with UV-excited laser-inscribed silver clusters. These results demonstrate the ability to perform efficient resonant non-radiative energy transfer from excited silver clusters to Eu^{3+}, allowing such energy transfer to be highly localized on demand thanks to laser inscription. Such results open the route to 3D printing of the rare earth ions emission in glass.

Keywords: silver clusters, rare earth ions, femtosecond laser inscription, FLIM spectroscopy, resonant transfers, Dexter process, FRET process, CIE chomaticity diagram

INTRODUCTION

Photonics has been clearly identified as a key enabling technology. The development of such penetrating technology relies on its ability to integrate and miniaturize components and devices. Therefore, the development of innovative materials together with the fabrication processes remain a central issue. Glass materials have shown, thanks to the development of fiber technology for instance, that they are excellent candidate for optical applications. New solution should found for enhancement and promoting 3D architectures. It requires developing intense local physical effect that could be structured in 3D. Direct laser writing are offering numerous solutions for shaping and inscribing functionality in Glass [(1)]. Moreover, especially designed glass composition can offer additional possibility for implementing multiple functionalities such as luminescence for instance [(2)]. Still now, structuring efficient emission in various spectral range remains an important challenge. This last decade, we demonstrated that

femtosecond direct laser writing (DLW) in a high optical quality photosensitive silver-containing zinc phosphate glasses allows for implementing 3D fluorescent structure formed by the aggregation of silver ions and silver atoms within the glass volume [(3)] that could be a solution for perennial three-dimension high-density data storage [(4)-(7)]. The cluster exhibit a broad excitation spectrum from 280 nm up to at least 550 nm. This local precipitation of silver cluster is preceded by the localized creation of a space charge separation at the root of a perennial high-amplitude (~10^{8-9} V/m) static electric field, leading to the local breaking of centrosymmetry and thus allowing for an efficient electric-field induced second-harmonic generation ($\chi^{(2)}_{eff}$ ~ 0.8 pm/V) [(9),(10)]. Moreover, the spatial structuring of the incident laser beam led us to achieve the first demonstration of bulk structuring by means of optical vortex-induced DLW [(11)], locally producing correlative optical contrast in terms of silver cluster fluorescence and of effective second-order nonlinear optical properties. Finally, these innovative laser-induced multi-scale structures were tuned into silver metallic nano-crystallites by means of thermal annealing, creating a composite metal-dielectric material with plasmonics properties [(12)]. The local cluster formation by DLW was recently shown to be partially or fully inhibited by original dual-color DLW with the co-illumination of a CW UV beam with the fs IR structuring beam, opening interesting potentialities in terms of super-resolution DLW [(8)]. The co-doping of glasses with both rare earth ions and noble metal ions has been increasingly reported [(13)-(16)], for optoelectronic devices such as white light emitting diode, three-dimensional display and solar cell [(13),(15)-(18)]. Indeed, efficient energy transfer between silver species and europium ions was described and achieved in various materials such as glasses and zeolite materials [(13),(14),(19)-(24)]. In glasses, beside the traditional melt technique to incorporate silver species with rare ions, different methods of preparation was described, such as the ion-exchange processes. The modification of the quantum yield of fluorescence emission has been described thanks to the presence of silver cluster and silver nanoparticles [(13)]. An enhancement of the rare earth emission by energy transfer from silver clusters to Eu^{3+} ions have been observed in various matrices such as in silicate [(20),(21)] or borate [(25)].

In most of the investigations there are no control on the spatial distribution of the rare earth ions emission and the 3D organization of the luminescent structure is not considered. In the specific case of photonic integrated circuits, the issue of the 3D organization of robust luminescent structure is crucial. The goal is then not solely the efficiency of the luminescent structure but also the engineering of luminescent 3D photonic structure. It requires to be able to foster locally efficient transfer or enhancement mechanisms between noble ion based aggregates and rare earth ions as for instance between silver species and europium ions.

In this article, we report on the co-doping of a silver-doped zinc phosphate glass with Europium Eu^{3+} rare earth ions and the 3D structure of the luminescent properties. The absorption, excitation and emission properties of the pristine co-doped glasses were investigated and micro-luminescence properties were characterized after femtosecond laser direct writing and the local precipitation of fluorescent silver clusters. The origin of the interaction between the silver clusters and the europium ions has been investigated in order to elucidate the potential contributions of radiative and non-radiative transfers. A local field enhancement effect due to hypothetical formation of metallic nanoparticles, is also discussed.

EXPERIMENTAL SECTION

Glass synthesis and sample preparation. The europium-doped silver-containing zinc phosphate glass with the composition 99.2[54.1 $PO_{5/2}$ / 37 ZnO / 1.4 $GaO_{3/2}$ / 7.5 $AgO_{1/2}$] - 0.8 Eu_2O_3 (mol. %) was prepared using classical melt/quench technique using platinum crucible. After annealing at 30°C below the glass transition temperature the glass is cut to 1 mm thick sample with typically 1 cm lateral dimensions and polished to optical quality. Hereafter, the co-doped glass sample is referred to as PZn:Ag-Eu. For nanoparticles development effect investigation, the glass was heat-treated at 400 °C, typically 20 °C above the glass transition temperature for 30 minutes.

Transmission, excitation and emission spectroscopies. The transmission spectroscopy was performed with a Carry 500 (differential transmission spectrometer from Varian) from 250 nm to 800 nm. The excitation and emission spectroscopies were performed with a SPEX Jobin Yvon fluorescence spectrometer equipped with double monochromator and Peltier cooled PMT.

Femtosecond direct laser writing. DLW was performed using a Ytterbium fs oscillator (Amplitude Systèmes, T-pulse 200, 9.1 MHz, 390 fs at 1030 nm), focused with a microscope objective (Mitutoyo, M Plan Apo NIR, 20× NA 0.4). The transmitted irradiances were controlled by an acousto-optic modulator, enabling focused energies up to 100 nJ and associated focused irradiances up to 20 TW/cm^2. The positioning and displacement of the sample were performed with a high-precision 3D translation stage (XMS-50 stages, Micro-Contrôle). A laser-matter interaction matrix was performed, by producing to 18 structured squares, each composed of 10 lines of 100 µm spaced by 10 µm, associated to 6 irradiances spanning from 2 to 6.7 TW/cm^2, and 3 translation speeds of 10, 50 and 100 µm/s, respectively corresponding to the local accumulation of 3.1×10^6, 6.2×10^6 and 3.1×10^5 pulses.

Absorption micro-spectroscopy of the structured sample. Transmission measurements were performed in bright-field using a 'CRAIC Technologies' microscope equipped with a Xenon lamp and a condenser as a white light source and with a spectrometer equipped with CCD . A conjugated 10x magnification microscope objective was used to collect the transmitted light through the laser-induced structures. For such micro-transmission measurements, the reference spectrum was recorded through the pristine glass, exactly in the same geometrical conditions for the measurement through the laser-induced structures, which excludes any artifacts from distinct collection issues. As a consequence the resulting transmission measurements gave a direct experimental access to the local differential micro-extinction due to the laser-induced structures. Such a local differential micro-extinction, interpreted in terms of linear absorption coefficient, is a spatially averaged value over a 50×50 µm^2 surface, successively overlapping each of the 100×100 µm^2 laser-induced structures.

Fluorescence micro-spectroscopy of the structured sample. Fluorescence spectrum measurements were performed in an epi-collection scheme, with a high spectral resolution micro-spectrometer (LabRAM HR800 from Jobin-Yvon, with a 150 grooves/cm grating for the spectral dispersion of the fluorescence in the near-UV and visible region) for three different conditions. First, a 325 nm excitation with a UV He-Cd laser source (30 mW, TEM 00 , Kimmon) was focused with a UV-enhanced Cassegrain objective (36× NA 0.5), and fluorescence was collected over the range of 330 nm – 750 nm. Second, a 405 nm excitation with a near-UV laser diode (100 mW, TEM00 , OBIS from COHERENT) was focused with a Olympus refractive objective (100× NA 0.9), and fluorescence was collected over the range of 450 nm – 750 nm. Finally, a 532 nm excitation with a laser diode (100 mW, TEM00 , monomode, Coherent) was focused with the same Olympus refractive objective (100× NA 0.9),

and fluorescence was collected over the range of 550 nm – 750 nm. Great care was taken to provide spectrally corrected fluorescence spectra for each of the three conditions.

Time-resolved fluorescence micro-spectroscopy of the structured sample. The Fluorescence Lifetime Imaging Microscopy (FLIM) analysis was performed with a Picoquant MT200 microscope equipped with two MPD single photon avalanche diodes (SPADs) and a PicoHarp300 timing board for Time Correlated Single Photon Counting (TCSPC) operation. The pulsed laser source was a frequency-doubled 6 ps coherent MIRA 900 laser, tuned at 435 nm, with a repetition rate set to 4.75 MHz via an acousto-optic pulse picker. The laser was reflected to a 100× 1.40NA oil objective (Olympus UPLSAPO100XO) by a 80%T/20%R spectrally flat beam splitter, and the fluorescence was collected by the same objective and transmitted by the same beam splitter to the confocal optics and detector after excitation light was rejected by a band-pass filter (HQ510/80, chroma with a 470-550 nm transmitted spectral window). The laser was scanned by means of a piezoelectric stage in a grid pattern of 156 nm steps and 0.6 ms/pixel. The shown FLIM images were calculated using the so-called "fast-FLIM" algorithm, where for each pixel, the reported lifetime was calculated as the first statistical momentum of the histogram distribution of the single photon arrival times, minus a reference time taken at the onset of the decay curve. Note that the shown FLIM images include both temporal and intensity information of the collected fluorescence, as the color code depicts the fast-FLIM average arrival times on the one hand and the brightness levels depicts the number of collected events on the other hand. Alternatively, curve fitting with a multi-exponential model was performed on decays with better statistics, corresponding to the binning of pixels of larger regions of interest. In the latter case, tail fitting could be applied thanks to the shortness of the instrumental response function (about 40 ps FWHM).

RESULTS AND DISCUSSION

Photoluminescence in Bulk Glass. The absorption spectrum in the range 250-800 nm obtained for the PZ: Ag/Eu^{3+} glass is shown in Figure 1. The UV edge is around 270 nm mainly due to silver ions absorption as previously observed for silver ions containing zinc phosphate glass [(26)]. Additional characteristic absorption bands of Eu^{3+} ions are observed at 318, 362, 380, 393, 464 and 526 nm assigned to the transition from the ground state $^7F_0$ to excited states $^5H_3$, $^5D_4$, $^5G_2$, $^5L_6$, $^5D_3$, $^5D_2$, respectively. There is no evidence of Eu^{2+} formation in the glasses and no absorption band above 300 nm, which could be attributed to surface plasmon resonance or silver cluster species such as $(Ag_2)^+$ or $(Ag_3)^{2+}$ for instance.

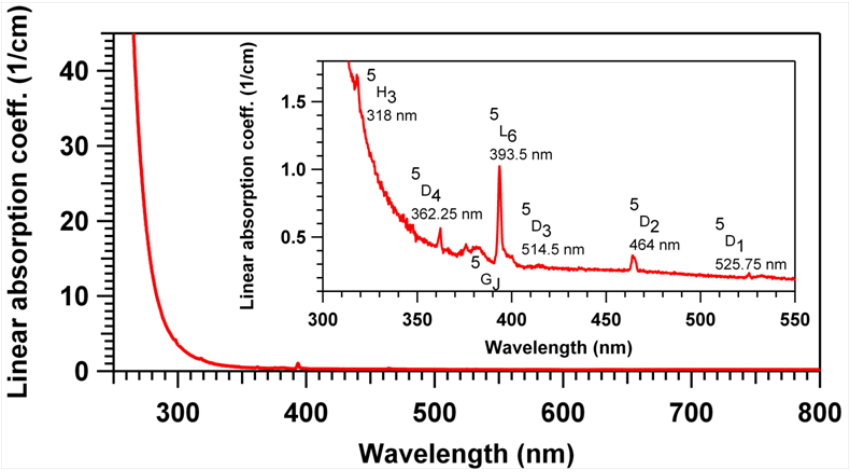

Figure 1. Linear absorption coefficient of the pristine PZ:Ag-Eu glass, mostly showing the UV cut-off due to the silver ion insertion below 300 nm, as well as the much weaker and narrow 4f-4f transition lines of the Eu^{3+} ions (see insert).

Fluorescence spectroscopy have been measured under different UV excitation wavelengths to investigate the emission properties of silver and Eu^{3+} ions and the results are shown in Figure 2(a). Under 235 nm excitation, two broad emission bands are observed due to two different intrinsic environments of silver with peak emission at 290 nm (site A) and 380 nm (site B), as well as the characteristics emissions of the 4f-4f transitions of Eu^{3+}: $^5D_0$-^7F_j (J=0-6). The site A emission is assigned to Ag^+ ion with the $^3D_J \rightarrow {}^1S_0$ transition, while site B emission is assigned to $(Ag^+)_2$ pairs with the $S_1, T_1 \rightarrow S_0$ transition [(27)]. Note that the considered silver ion concentration makes site B is largely preponderant compared to site A [(2)]. With the increase of the excitation wavelength to 260 nm, almost exclusively site B emission as well as the characteristics emission of Eu^{3+} is observed. Excitation at UV light about 235 nm or 260 nm, promotes the electron to the excited state of both sites A and B, or site B, respectively. Thus, the excited electrons can relax to the ground state radiatively, but also non-radiatively including relaxation paths involving energy transfers to the neighboring Eu^{3+} ions. The occurrence of energy transfer from silver sites to Eu^{3+} ions is favored by the energy level accordance between the excited states of the silver sites with the $^5L_6$ level of Eu^{3+} ions. Under excitation at 365 nm, only the line-shape characteristics emissions of the Eu^{3+} transitions at 578 nm, 590 nm, 612 nm, 652nm and 702 nm corresponding to the Eu^{3+} ions emission $^5D_0 \rightarrow {}^7F_J$ (J= 0-4) are observed.

Based on the photoluminescence spectra of the glasses presented in Fig. 2, the color of samples under the three distinct excitations at 235 nm, 260 nm and 365 nm were characterized by International Commission on Illumination (CIE) chromacity diagram (Fig. 2b). The colors shift from purplish pink to red with the increase of excitation wavelength from 235 nm to 365 nm, which demonstrates that the luminescence color can be systematically tuned by changing the excitation wavelength.

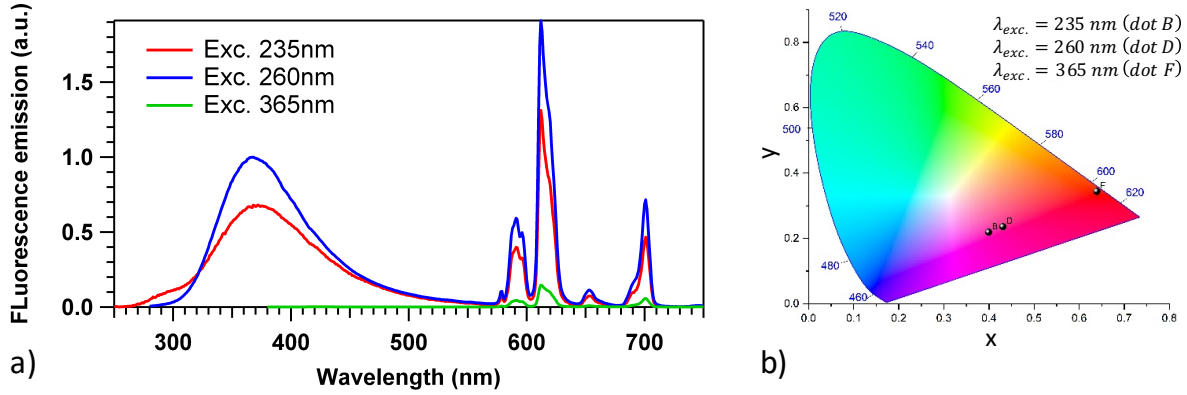

Figure 2. (a) Fluorescence emission spectroscopy of the pristine PZ:Ag-Eu sample for three distinct excitation wavelengths, showing two broad emission bands of two distinct environments of the silvers ions, labeled site A (exc. 235 nm and em. 290 nm, lower amplitude) and site B (exc. 260 nm and em. 380 nm, larger amplitude), as well as the emission of the 4f-4f transitions from the $^5D_0$ level of the Eu^{3+} ions (left). Note that the excitation at 365 nm is selective of the Eu^{3+} excitation, compared to the excitation of the Ag^+ ions. (b) CIE chromaticity diagram of the pristine PZ:Ag-Eu sample for three distinct excitation wavelengths.

The photoluminescence excitation spectra is shown in Figure 3. By monitoring the emission at 290 nm (site A), a broad excitation band centered at 230 nm is observed attributed to Ag^+ ion. At 340 nm (site B), two overlapping broad excitation bands are observed centered

at 230 nm and 260 nm, from the Ag^+ ion and $(Ag^+)_2$ pairs, respectively. When monitoring the Eu^{3+} emissions at 612 nm or 700 nm, besides the two broad excitation bands of silver originating from the energy transfer of Ag^+ ions and $(Ag^+)_2$ pairs energy transfer to the rare earth ions, several characteristic f-f transitions sharps lines are observed. Under UV-light, Ag^+ ions and $(Ag^+)_2$ pairs can be excited to the ^3D_j and S_1 energy levels, respectively, and then the non-radiative $S_1 \rightarrow S_0$ and $^3D_J \rightarrow S_0$ transitions may transfer the excitation energy non-radiatively to Eu^{3+} ions, such populated Eu^{3+} excited levels leading then to the observed typical Eu^{3+} fluorescent emission. Such non-radiative energy transfer is understood as a non-radiative resonant relaxation from the Silver species (donor) to the Eu^{3+} ions (acceptor), without any electron transfer. Indeed, the overlapping of excitation bands evidences the potential ability of energy transfer from silver ionic species to the Eu^{3+} ions. Furthermore, no fluorescence emission signature of Eu^{2+} ions was observed, which corroborates the absence of electron transfer in the present energy transfer.

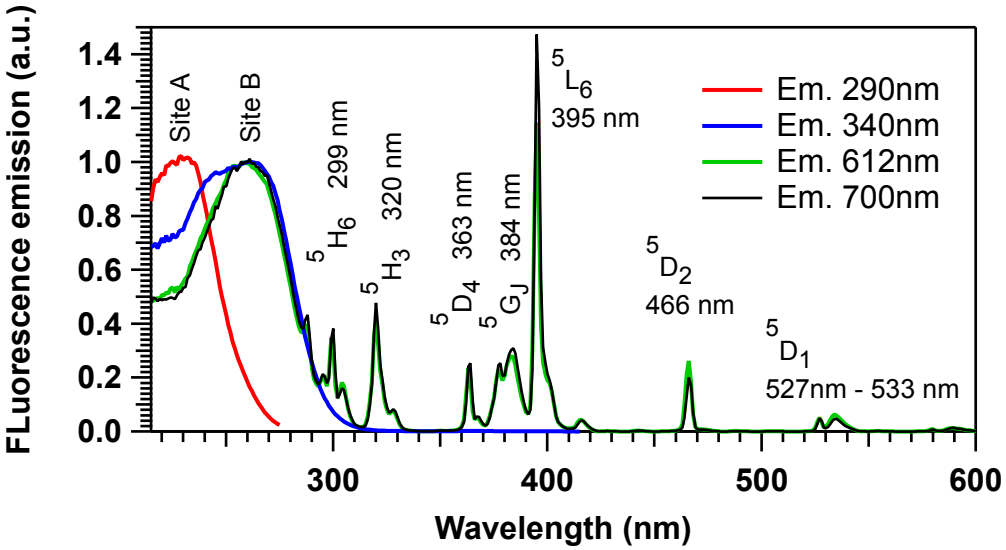

Figure 3. Fluorescence excitation spectroscopy of the pristine PZ:Ag-Eu sample for three distinct emission wavelengths, showing two broad excitation bands of two distinct environments of the silvers ions, labeled site A (exc. 235 nm and em. 290 nm) and site B (exc. 260 nm and em. 380 nm), as well as the excitation of the 4f-4f transitions of the Eu^{3+} ions.

Direct Laser Writing of Fluorescence Structures. Figure 4(a) shows a wide-field fluorescence microscopy image of coil patterns obtained by DLW for PZ:Ag-Eu glass sample motion with controlled speed from 10 to 100 µm/s (corresponding to C, B and A lines), and for different irradiances from 4.0 to 6.7 TW cm^{-2} (labeled columns 3, 4, 5 and 6). Those pattern allow investigating the influence of the laser parameters in the silver clusters growth and their interaction with the Eu^{3+} ions. A high-resolution confocal image for excitation 435 nm (obj. 100x NA1.4) is given in Fig. 4(b), showing the detailed distribution of the fluorescent double-line structure produced by several laser passes. These double lines correspond to the formation of parallel planes containing the silver clusters at the border of the voxel of interaction. This phenomenon has been described in details elsewhere [(4)].

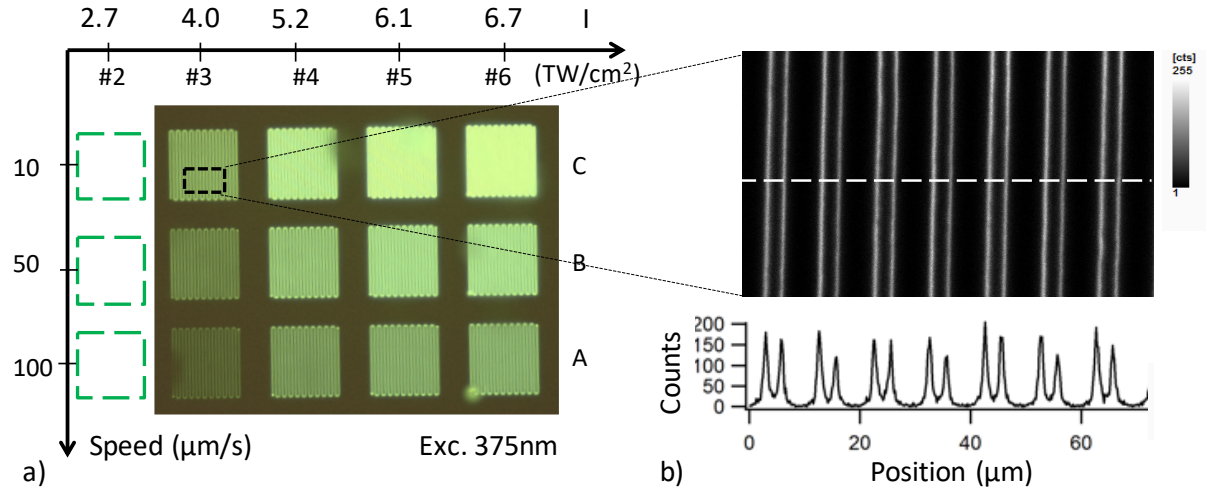

Figure 4. Laser/matter interaction matrix: (a) wide-field fluorescence microscopy (Obj. 20x NA0.4, excitation at 375 nm), revealing the laser-induced fluorescence of the 100x100 µm^2 patterns after DLW; (b) confocal microscopy imaging (oil obj. 100x NA1.4, excitation 435 nm, collection from 470 nm to 550 nm), zooming a part of the pattern C3 (10 µm/s, 4 TW/cm^2) revealing in detail the fluorescent double-line structure inscribed at each laser pass: insert below the image shows the 1D horizontal cross-section of the high-resolution image along the dashed line.

Micro-absorptions measurements were performed in transmission mode both in a pristine area of the glass and in structures zones over a 50×50 µm^2 surface giving a direct experimental access to the local differential micro-absorption due to the laser-induced structures. They are presented in Figs. 5(a) and 5(b) for speed of 10 and 100 µm/s, respectively. These spectra have been decomposed by gaussian contributions. Two contributions have been observed around 335 nm (3.7 eV) and around 285 nm (4.35 eV). These two contributions increase in intensity with the irradiance and decrease in intensity with the speed. As can be seen, the relative intensity of these two bands are modulated by the dose deposition indicating that several centers are formed during the DLW process. The strongest dose tend to favor the absorption band around 335 nm (3.7 eV).

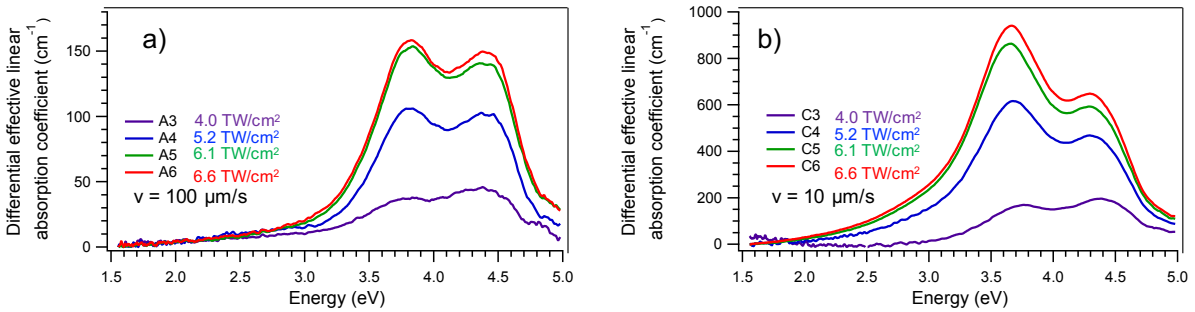

Figure 5. Micro-absorption spectroscopy of the laser/matter interaction matrix for laser-induced squares, observed with a 50×50 µm^2 field of view, showing the spatially-averaged differential linear absorption coefficient with respect to the pristine glass, revealing the creation and growth of two mains absorption bands (typically centered at 3.7 eV and 4.35 eV nm, depending on irradiation conditions) with respect to the laser irradiance at constant speed translations of (a) 10 µm.s^{-1} and (b) 100 µm.s^{-1}.

The micro-emission spectroscopy of laser induced silver clusters are presented in Figure 6 for two different excitations wavelengths at 325 nm and 405 nm as a function of the sample motion velocity for 6.75 TW.cm^{-2} irradiance (Fig. 6a and 6c) and as a function of the irradiance for a fixed sample motion velocity of 10 µm/s (Fig. 6b and 6d).
At 325 nm (Figs. 6a and 6b), the emission spectra consist of two major contributions, one broad emission ranging from 400 to 700 nm attributed to silver nanoclusters and sharp emission peaks within the 575 to 715 nm region assigned to Europium ions. The decrease in sample velocity (Fig. 6a) and the increase of the irradiance (Fig. 6d) corresponding to a raise of the deposited dose promote the increase of the broad emission band intensity assigned to the formation of Ag_m^{n+} species and promote also the emission of the europium ions. The most intense emission of Eu^{3+} around 612 nm is attributed to the hypersensitive electric dipole transition ($^5D_0 \rightarrow {}^7F_2$). This emission is strongly influenced by the chemical environment of the Eu^{3+} ions in the host network. On the other hand, the $^5D_0 \rightarrow {}^7F_1$ transition occurs via the magnetic dipole mechanism and its intensity is not sensitive to the chemical environment of Eu^{3+} ions. Therefore, the emission intensity ratio of these two transitions can be used to highlight a site evolution of the rare earth ion. In the present case, one can notice that the spectral shape of the 4f-4f transition remains constant and the intensity ratio between the $^5D_0 \rightarrow {}^7F_2$ and $^5D_0 \rightarrow {}^7F_1$ also remains at constant value of 4.1 ± 0.1. Thus an absence of major modification of the chemical environment at the vicinity of the Eu^{3+} after DLW can be assumed.

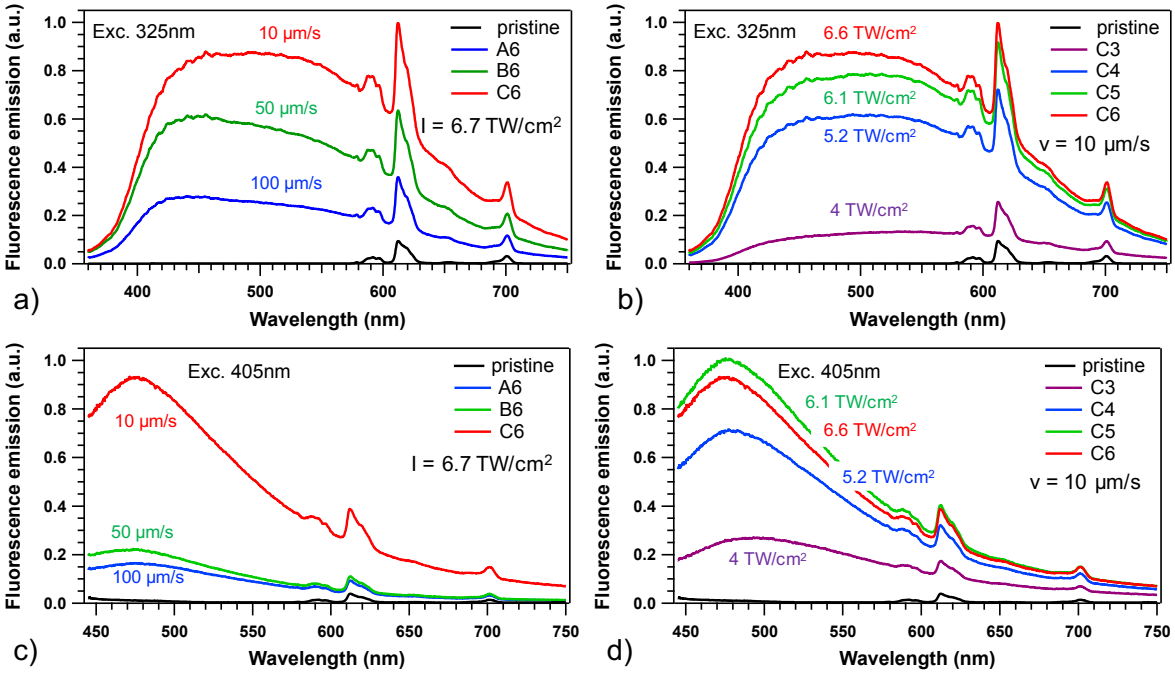

Figure 6: Micro-emission fluorescence spectroscopy of the laser/matter interaction matrix for some laser-induced squares. Excitation at 325 nm (reflective obj. 36x, NA 0.4): (a) dependence with sample translation velocity (irradiance = 6.7 TW/cm^2), and (b) dependence with irradiance (translation velocity = 10 µm/s). Excitation at 405 nm (refractive obj. 100x, NA 0.9): (c) dependence with sample translation velocity (irradiance = 6.7 TW/cm^2), and (d) dependence with irradiance (translation velocity = 10 µm/s).

Micro-fluorescence emission spectra bring interesting behavior in terms of display and colorimetry. Indeed, the fluorescence emission analysis under UV excitation at 325 nm and associated projection in the XYZ tri-chromatic coordinates in the CIE chromaticity diagram shows that the chromatic coordinates can be continuously controlled in 3D by means of laser irradiation, namely from red (almost pristine glass with quasi-null action of the laser inscription)

to white light emission, as shown in Fig. 7. In the case of the largest irradiances (I = 6.7 TW/cm^2 for patterns A6, B6 and C6 depicted in Fig. 7(a)), the trichromatic coordinates get very localized in the white emission domain whatever the three used velocities suggesting that the broadband silver cluster emission dominates the reddish contribution of Eu^{3+} ions in the resulting tri-chromatic behavior. Similarly, in the case of the lowest velocity v = 10 µm/s (namely, the largest number of cumulated pulses with patterns C3 to C6 depicted in Fig. 7(c)), the deposited dose is also high enough to produce enough efficient fluorescent silver clusters to overcome the Eu^{3+} emission and dominate the resulting tri-chromatic behavior. However, a larger velocity of 50 µm/s tends to limit the amount of silver clusters and its fluorescence emission amplitude, locally allowing for a control a the tri-chromatic coordinates between the initial red coordinates of the pristine glass and the white light emission of the silver clusters, as show between points B2 and B3 from Fig. 7(b). Such measurements results from micro-luminescence in confocal microscopy, so that there are measured at the silver cluster positions. By adjusting the probed volume of the material of the one hand, and by fixing the filling rate of silver cluster (typically with the inter-distance between successive laser passes in a given plane, or by producing thick multi-plane patterns) on the other hand, one can fully control the continuous evolution of the measured tri-chromatic coordinate between red to white emission. This suggest thus the ability to perform the localized 3D inscription of emitting areas with tunable tri-chromatic coordinates, which goes beyond the spatially homogeneous control of the tri-chromatic coordinates means of selecting different fluorescence excitations wavelengths as shown in Fig. 2(b) (from the pristine Eu^{3+}-based red emission to a pinkish emission resulting from the red Eu^{3+} ion emission and the blue Ag+ ion emission in the pristine glass). Laser inscription allows thus an additional experimental parameter to tune the 3D localized tri-chromatic coordinates.

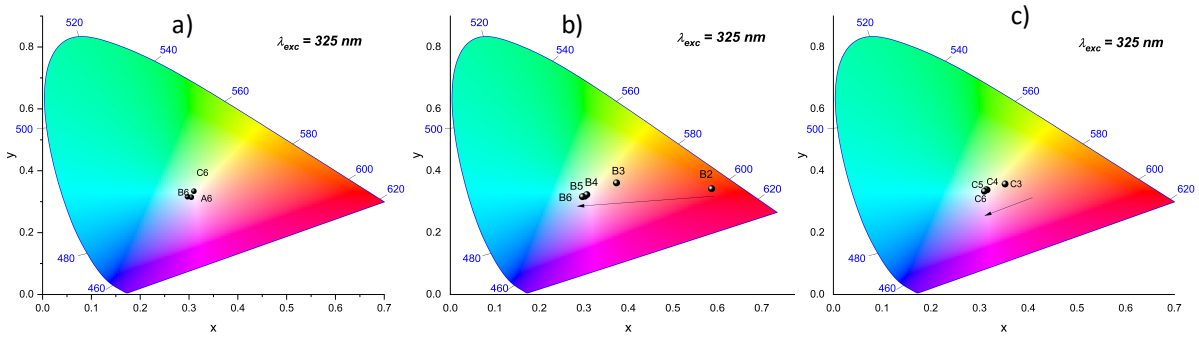

Figure 7. CIE chromaticity diagram of the laser/matter interaction matrix for some laser-induced squares with excitation at 325 nm.

To further investigate the energy transfer from silver clusters to Eu^{3+} ions, time-resolved spectroscopy of silver nanocluster emission was obtained for the PZ:Ag and PZ:Ag:Eu glasses, for a collection over the 470-550 nm spectral range and using a pulsed excitation (6 ps, 4.75 MHz) at 435 nm. The collected fluorescence predominantly corresponds to that of silver clusters, because Eu^{3+} ions show no emission in this spectral range and because Ag^+ ions of the glass matrix show negligible fluorescence excitation. In these conditions, Figs. 8(a) and 8(b) show the FAST-FLIM images for the laser inscribed patterns, where the color code and the brightness depict the pixel-to-pixel FAST-FLIM average lifetime and the associated fluorescence intensity, respectively. For both the PZ:Ag and PZ:Ag:Eu glasses, the FAST-FLIM images corroborate the double-line spatial distribution of laser-induced fluorescent silver clusters, as shown in Fig. 4. The intensity weighted FAST-FLIM lifetime histograms were extracted from Figs. 8(a) and 8(b), and have been reported in Fig. 8(c). These histograms clearly show the mean lifetime shortening of the silver cluster excited states in the presence of Eu^{3+} ions, with a typical peak value of the histograms occurring at a shorter lifetime of 1.94 ns for

the PZ:Ag:Eu glass, compared to the 2.44 ns lifetime for the PZ:Ag glass. This supports the hypothesis of a quenching by energy transfer from these clusters to the neighboring Eu^{3+} ions which directly affect the emission rate of the cluster emission. Figure 8(c) also reveals a lower emission intensity of silver clusters in the presence of Eu^{3+} ions, such partial emission quenching being also consistent with nonradiative energy transfer by resonant energy transfer from silver clusters to Eu^{3+} ions. By properly taking into account the normalization with the incident pump intensity at 435 nm for both histograms of Fig. 8(c), the corresponding time-integrated intensity of both PZ:Ag and PZ:Ag:Eu glasses led to the intensity quenching $Q_{I_{Ag,Eu}^{fluo} / I_{Ag}^{fluo}} = 1 - I_{Ag,Eu}^{fluo}/I_{Ag}^{fluo} \sim 41\%$ of the silver cluster emission. Note that such global intensity quenching includes any sources of quenching, namely the energy transfers at play towards the Eu^{3+} ions but also others possible phenomena whose contributions will be discussed below.

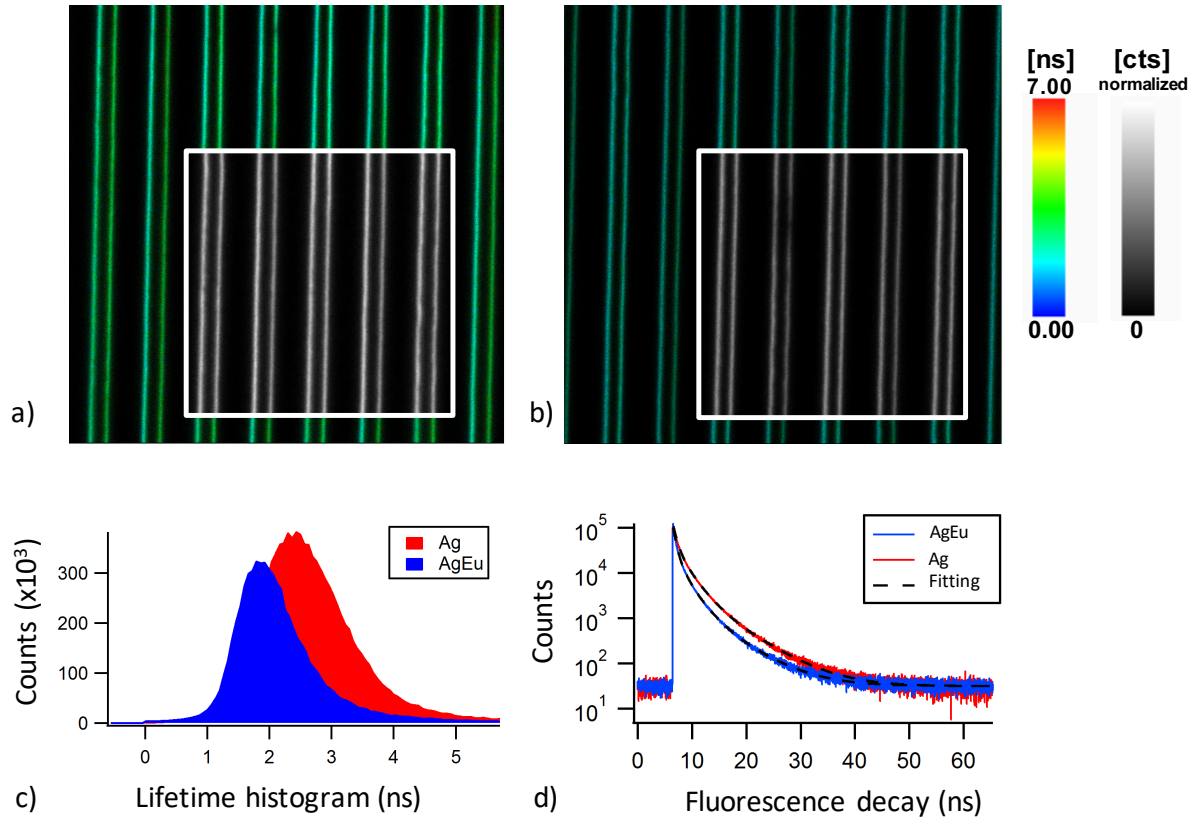

Figure 8: (a) Composite image of the laser-induced pattern C3 (10 µm/s, 4 TW/cm^2) in the PZn:Ag glass depicting a color image of the laser that provides the pixel-by-pixel mean lifetime retrieved by fast-FLIM algorithm (see color bar from 0 to 7 ns), as well as a grey-scale inset image (see color bar from 0 to 255 counts) that provides the fluorescence intensity; (b) same composite image FLIM and fluorescence intensity for the PZn:Ag:Eu glass; (c) Intensity-weighted lifetime histograms for the PZn:Ag and PZn:Ag:Eu glasses obtained from the FLIM images depicted in 8(a) and 8(b), respectively; and (d) normalized fluorescence decays of both the PZn:Ag and PZn:Ag:Eu glasses and their ideal respective fittings with a four independent exponential decay model. All data was obtained with a 435 nm pulse excitation of 6 ps at 4.75 MHz, and a collection over the 470-550 nm range.

As the fluorescence emission of the silver clusters corresponds to a broadband multi-band emission that covers the whole visible range and depends on laser irradiation parameters, fluorescence lifetime was also evaluated with a multiple exponential decay model in the sub-ns

and ns range. As detailed in the experimental section, curve fitting with a multi-exponential decay model was performed on decays with better statistics, corresponding to the binning of pixels of larger regions of interest. As shown in Fig. 8(d), optimal time decay fitting was achieved with a four-exponential model with the adjusted amplitudes and time constants being reported in Table 1. The used model demonstrates that the complexity of lifetime decay of the system under investigation requires at least four typical decay times, but reality may even be more complex with additional much shorter decay times.

PZnAg	τ_i (ns)	A_i (cts)	A_i (%)	PZnAg:Eu	τ_i (ns)	A_i (cts)	A_i (%)
Exp. #1	6.25	3527	3.3	Exp. #1	5.75	2259	2.3
Exp. #2	2.67	19008	17.7	Exp. #2	2.19	16645	17.2
Exp. #3	1.48	24017	22.4	Exp. #3	0.92	25573	26.5
Exp. #4	0.58	60861	56.7	Exp. #4	0.42	52047	53.9

Table 1: Fitting parameters with a four-exponential decay time model.

Based on the fitting results from Table 1, the intensity-weighted average emission lifetime $\tau^{int.} = (\sum_{i=1..4} A_i\tau_i^2)/(\sum_{i=1..4} A_i\tau_i)$ is of $\tau_{Ag}^{int.}$ = 2.44 ns for the PZ:Ag glass and it decreases down to $\tau_{Ag,Eu}^{int.}$ = 1.94 ns in the Eu^{3+}-containing glass, in agreement with the lifetimes denoted by the peak positions of the histograms of Fig. 8(c). This result corroborates the occurrence of energy transfer from Ag_m^{n+} species levels to Eu^{3+} ions. Accordingly to the expected lifetime of europium Eu^{3+} in such glass, which is expected to be around the millisecond for the most intense emission around 612 nm, the collected decay measurement strictly corresponds to the silver cluster contribution.

To go further in the interpretation of energy transfers, based on the fitting results from Fig. Table 1, the amplitude-weighted average emission lifetime $\tau^{ampl.} = (\sum_{i=1..4} A_i\tau_i)/(\sum_{i=1..4} A_i)$ has also been estimated, leading to $\tau_{Ag}^{ampl.}$ = 1.34 ns and to $\tau_{Ag,Eu}^{ampl.}$ = 0.98 ns for the PZ:Ag and PZ:Ag:Eu glasses, respectively. The amplitude-weighted quenching rate $Q_{\tau_{Ag,Eu}^{ampl.}/\tau_{Ag}^{ampl.}}$ of the emitting silver clusters can be estimated as $Q_{\tau_{Ag,Eu}^{ampl.}/\tau_{Ag}^{ampl.}} = 1 - \tau_{Ag,Eu}^{ampl.}/\tau_{Ag}^{ampl.} \sim 27\%$. The comparison of the amplitude-weighted quenching rate $Q_{\tau_{Ag,Eu}^{ampl.}/\tau_{Ag}^{ampl.}} \sim 27\%$ with the intensity quenching rate $Q_{I_{Ag,Eu}^{fluo}/I_{Ag}^{fluo}} \sim 41\%$ helps sorting the contributions of the emission quenching of the silver clusters. Indeed, the ratio $Q_{\tau_{Ag,Eu}^{ampl.}/\tau_{Ag}^{ampl.}}/Q_{I_{Ag,Eu}^{fluo}/I_{Ag}^{fluo}} = 27\%/41\% \sim 66\%$ indicates that 66% of the emission quenching of the silver clusters in presence of Eu^{3+} ions is actually due to energy transfer. In addition, the estimation $1 - Q_{\tau_{Ag,Eu}^{ampl.}/\tau_{Ag}^{ampl.}}/Q_{I_{Ag,Eu}^{fluo}/I_{Ag}^{fluo}} \sim 33\%$ indicates that 33% of the emission quenching of the silver clusters in presence of Eu^{3+} ions stands either for a lower concentrations of Silver emitters, affecting the fluorescence intensities but not the lifetimes. This can reasonably be interpreted by a slightly lower efficiency of silver cluster production during the femtosecond laser writing process. Indeed, in the laser inscription stage, we observed that Eu^{3+} ions undergo multi-photon absorption and subsequent reddish fluorescence emission, which partially reduces the effective femtosecond laser intensity and thus competes the activation of the silver photochemistry and the associated creation and growth of silver clusters.
Regarding the Europium emission intensity, the 612 nm Eu^{3+} emission increases up to 5-fold and to 3.5-fold for excitations at 325 nm and 405 nm, respectively (Figs. 9(a) and 9(b)), indicating an energy transfer from silver species to Eu^{3+} ions [(17),(23),(25)]. The Eu^{3+} emission

enhancement is clearly dependent with the excitation wavelength as a larger efficiency is observed for an excitation at 325 nm. Such wavelength excitation dependence may be directly interpreted from Fig. 5, with a more efficient excitation of silver clusters at 325 nm compared to 405 nm, leading thus to a more intense fluorescence emission and consequently to a larger amount of excited silver clusters compatible with resonant non-radiative energy transfers to Eu^{3+} ions. Still, the existence of various populations of distinct silver clusters created during DLW has been yet reported [(12)], showing a partially-selective excitation with radiations at 325 nm or 405 nm which may also play a selective role if the observed energy transfer. Indeed, these distinct types of silver clusters may show distinct energy transfer efficiencies to the Eu^{3+} ions. The present spectroscopy cannot directly identify the nuclearities and associated stabilized Redox charges of these silver species, nor their respective populations [(12)].

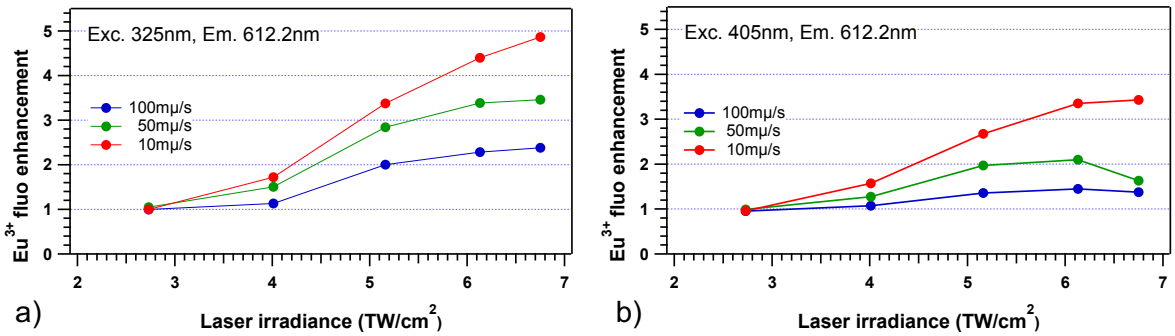

Figure 9: Normalized amplitude of the micro-emission of the Eu^{3+} fluorescence with respect to the pristine glass at 612.2nm, (a) for a 325 nm excitation and (b) for a 405 nm excitation, respectively showing up to 5-fold and to 3.5 emission enhancements.

According to the singlet-triplet energy level model of Ag_m^{n+} species proposed by Velazquez et al. [(27)] and to the results obtained from the photoluminescent excitation and emission spectra of the Eu^{3+} and Ag_m^{n+} species in the co-doped glass before and after laser/matter interaction, the energy transfer pathway was tentatively described in Fig. 10. Under UV-visible, Ag^+ ions and Ag_m^{n+} species can be excited to the S_1 and T_2 energy levels, and then the $S_1 \rightarrow S_0$ and $T_2 \rightarrow S_0$ transitions may transfer the excitation energy to Eu^{3+} by relaxations, populating thus the $^5H_3$ level and by non-radiatively relaxing from the $^5D_4$ and $^5L_6$ levels down to the $^5D_0$ energy level. The subsequent radiative transitions from the $^5D_0$ energy upper level leads to the visible Eu^{3+} emissions observed in Figs. 2 and 6. Besides, it is worth to mention that the spin-forbidden transition of $T_2 \rightarrow S_0$ with relatively longer lifetime may mainly contribute to the above energy transfer processes. Still, at this level of description, the present spectroscopy cannot directly identify the mechanisms at play during the non-radiative resonant energy transfers, namely one cannot directly discriminate between Dexter resonant energy transfers (DET) related to electron exchange operating at very short scale (requirement of the wave function overlap) or Förster resonant energy transfers (FRET) related to dipole-dipole interactions spanning over longer scales possibly up to several nanometers typically (but highly sensitive to the solicited oscillation strength, which is known to rather weak for the lanthanide ions) [(28)]. A balance between DET and FRET both occurring simultaneously may even exist. Such discrimination in the origin of the involved resonant energy transfer could further be addressed thanks to a set of glasses with various rare earth doping concentrations, which is beyond the scope of the present article.

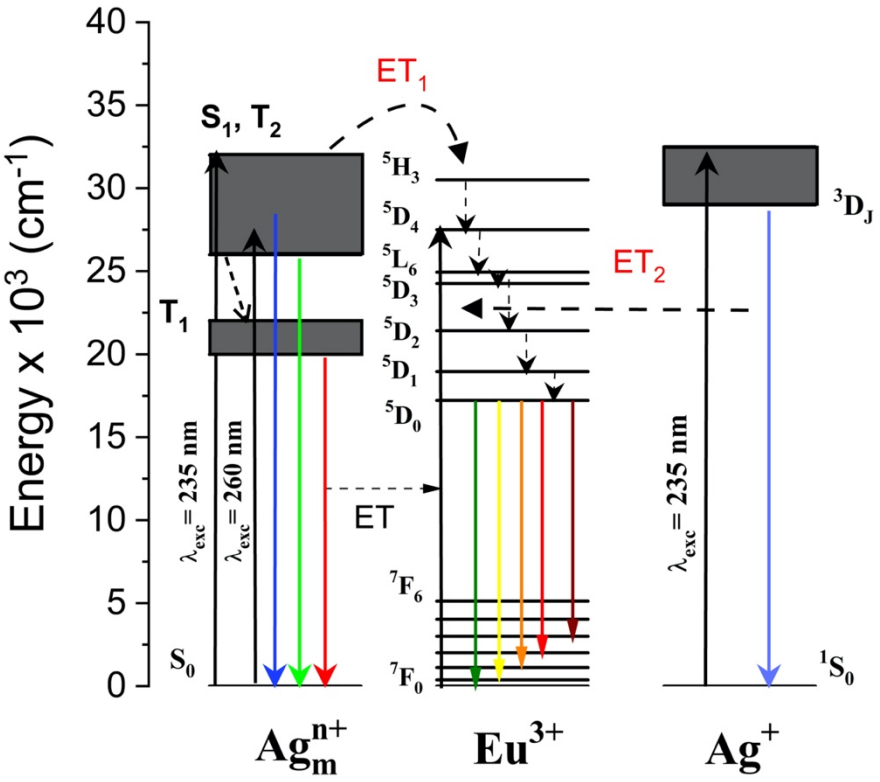

Figure 10. Energy level diagram showing schematically the possible energy transfer processes from Ag_m^{n+} to Eu^{3+} (energy transfer labelled ET_1), and from Ag^+ to Eu^{3+}(energy transfer labelled ET_2), upon excitation in the ultraviolet or visible range, leading to silver species emissions but also the indirect excitation of Eu^{3+} and its emission in the visible.

Following the laser/matter interaction a subsequent heat treatment done at 400 ºC (T_g+20°C) for 30 min in the glass revealed the crystallization of plasmonic silver nanoparticles. Such plasmonic structure precipitation will not be described in detail the present paper, as they were investigated earlier by Marquestaut *et al.* [(12)]. These plasmonic structures led to a quenching of the energy transfer between Ag species and Eu^{3+} ions, so that the enhancement of the Eu^{3+} emission mostly cancelled after thermal treatment, as shown in Figure 11 for an excitation at 325 nm. Indeed, the Eu^{3+} emission enhancement ratio drops from 2.5 to 5-fold down to 1.2- to 1.8-fold (with an enhancement drop from 5-fold down to 1.2-fold for the highest laser-deposited dose from pattern C6). The precipitation of silver nanoparticles decreases the active population of silver clusters that can be excited and further transfer energy to Eu^{3+} ions, reducing thus the energy transfer ability. Additionally, such silver nanoparticles can also contribute to quench the fluorescence emission of the remaining silver clusters, reducing furthermore the probability of energy transfer to Eu^{3+} ions.

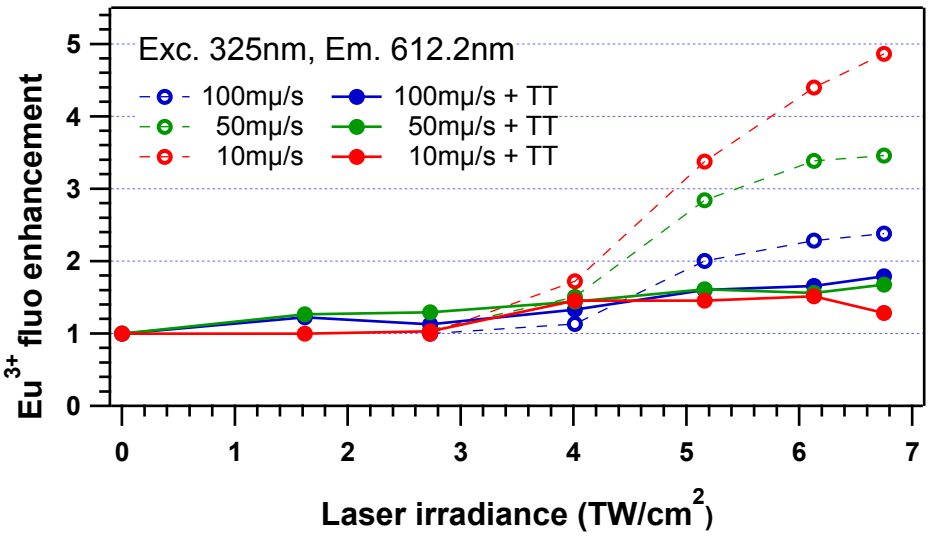

Figure 11. Normalized amplitude of the micro-emission of the Eu^{3+} fluorescence with respect to the pristine glass at 612.2nm, for a 325 nm excitation before (dashed line, empty dots) and after thermal heat treatment (TT) at 400 °C (T_g+20°C) for 30 minutes, showing both the decrease of the Eu^{3+} fluorescence enhancement for high enough deposited laser doses (partial growth and subsequent destruction of populations of initially large silver clusters and correlative growth of metallic plasmonic silver NPs) also well as the minor but non-zero increase of the Eu^{3+} fluorescence enhancement for lower deposited laser doses (partial growth from laser-induced defects or from populations of initially small silver clusters towards larger silver clusters that show a better resonant energy transfer toward Eu^{3+} electronic levels.

CONCLUSION

Femtosecond laser inscription was achieved in a Eu^{3+}-doped Silver-containing Zinc phosphate glass, demonstrating that the insertion of rare earth ions does not inhibit the photo-activation of silver chemistry. By means of micro-spectroscopy of fluorescence emission, tri-chromatic coordinates in the CIE chromaticity diagram were estimated showing that such coordinates can be continuously controlled from the red light aspect dominated by the Eu^{3+} emission towards the white light aspect dominated by the silver cluster emission. This demonstrated the ability to perform a 3D-localized controlled modification of the local tri-coordinates thanks to the laser irradiation parameters. Compared to the pristine, Eu^{3+} emission in the structured region showed an increase up to 5-fold and to 3.5-fold for excitations at 325 nm and 405 nm, respectively. Such an enhancement is co-localized with the fluorescent laser-inscribed silver clusters, which suggests a resonant non-radiative energy transfer from excited silver clusters to Eu^{3+} allowing then the fluorescence of the rare earth ion. FAST-FLIM imaging the efficient resonant energy transfer from the silver clusters and to Eu^{3+} ions. The precipitation of metallic silver plasmonic nanoparticles in the silver cluster location, obtained following a heat treatment above glass transition temperature, vanishes the enhancement of the Eu^{3+} emission. Femtosecond laser inscription in rare earth doped silver-containing glasses clearly demonstrates the effect of the silver cluster on the enhancement of europium ions and allows writing 3D localized intense tunable emission patterns from red to white for a broad excitation spectrum in inorganic materials. This approach could be extended to other rare earth doped photosensitive glasses, including photo-thermo-refractive glasses [(29)], to promote 3D high contrast luminescent pattern in various spectral ranges.

REFERENCES:

(1) Gross, S.; Withford, M. J.; Ultrafast-laser-inscribed 3D integrated photonics: challenges and emerging applications, Nanophotonics **2015**; 4:332–352.

(2) Petit, Y.; Danto, S.; Guérineau,T.; Khalil, A.A.; Le Camus, A.; Fargin, E.; Duchateau, G.; Bérubé, J.-P.; Vallée, R.; Messaddeq, Y.; Cardinal, T.; Canioni, L.; On the femtosecond laser-induced photochemistry in silver-containing oxide glasses: mechanisms, related optical and physico-chemical properties, and technological applications, Advanced Optical Technologies, 7 (5), 291-309 (**2018**).

(3) Royon, A.; Petit, Y.; Papon, G.; Richardson, M.; Canioni, L. Femtosecond Laser Induced Photochemistry in Materials Tailored with Photosensitive Agents [Invited]. *Opt. Mater. Express* **2011**. https://doi.org/10.1364/ome.1.000866.

(4) Bellec, M.; Royon, A.; Bourhis, K.; Choi, J.; Bousquet, B.; Treguer, M.; Cardinal, T.; Videau, J. J.; Richardson, M.; Canioni, L. 3d Patterning at the Nanoscale of Fluorescent Emitters in Glass. *J. Phys. Chem. C* **2010**. https://doi.org/10.1021/jp104049e.

(5) Royon, A.; Bourhis, K.; Bellec, M.; Papon, G.; Bousquet, B.; Deshayes, Y.; Cardinal, T.; Canioni, L. Silver Clusters Embedded in Glass as a Perennial High Capacity Optical Recording Medium. *Adv. Mater.* **2010**. https://doi.org/10.1002/adma.201002413.

(6) Canioni, L.; Bellec, M.; Royon, A.; Bousquet, B.; Cardinal, T. Three-Dimensional Optical Data Storage Using Third-Harmonic Generation in Silver Zinc Phosphate Glass. *Opt. Lett.* **2008**. https://doi.org/10.1364/ol.33.000360.

(7) Park, C.-H.; Petit, Y.; Canioni, L. and Park, S.-H. Five-dimensional high-density perennial optical data storage based on ellipse orientation and fluorescence intensity in silver-containing Zinc-phosphate glasses, MDPI Micromachines, *11*, 1026 (**2020**). doi:10.3390/mi11121026.

(8) Petit, Y.; Mishchik, K.; Varkentina, N.; Marquestaut, N.; Royon, A.; Manek-Hönninger, I.; Cardinal, T.; Canioni, L. Dual-Color Control and Inhibition of Direct Laser Writing in Silver-Containing Phosphate Glasses. *Opt. Lett.* **2015**. https://doi.org/10.1364/ol.40.004134.

(9) Papon, G.; Petit, Y.; Marquestaut, N.; Royon, A.; Dussauze, M.; Rodriguez, V.; Cardinal, T.; Canioni, L. Fluorescence and Second-Harmonic Generation Correlative Microscopy to Probe Space Charge Separation and Silver Cluster Stabilization during Direct Laser Writing in a Tailored Silver-Containing Glass. *Opt. Mater. Express* **2013**. https://doi.org/10.1364/ome.3.001855.

(10) Papon, G.; Marquestaut, N.; Petit, Y.; Royon, A.; Dussauze, M.; Rodriguez, V.; Cardinal, T.; Canioni, L. Femtosecond Single-Beam Direct Laser Poling of Stable and Efficient Second-Order Nonlinear Optical Properties in Glass. *J. Appl. Phys.* **2014**. https://doi.org/10.1063/1.4869058.

(11) Mishchik, K.; Petit, Y.; Brasselet, E.; Royon, A.; Cardinal, T.; Canioni, L. Patterning Linear and Nonlinear Optical Properties of Photosensitive Glasses by Femtosecond Structured Light. *Opt. Lett.* **2015**. https://doi.org/10.1364/ol.40.000201.

(12) Marquestaut, N.; Petit, Y.; Royon, A.; Mounaix, P.; Cardinal, T.; Canioni, L. Three-Dimensional Silver Nanoparticle Formation Using Femtosecond Laser Irradiation in Phosphate Glasses: Analogy with Photography. *Adv. Funct. Mater.* **2014**. https://doi.org/10.1002/adfm.201401103.

(13) Ma, R.; Gao, J.; Xu, Q.; Cui, S.; Qiao, X.; Du, J.; Fan, X. Eu2 + Promoted Formation of Molecule-like Ag and Enhanced White Luminescence of Ag/Eu-Codoped Oxyfluoride Glasses. *J. Non. Cryst. Solids* **2016**. https://doi.org/10.1016/j.jnoncrysol.2015.10.032.

(14) Guo, Z.; Ye, S.; Liu, T.; Li, S.; Wang, D. SmF3 Doping and Heat Treatment Manipulated Ag Species Evaluation and Efficient Energy Transfer from Ag Nanoclusters to Sm3 + Ions in Oxyfluoride Glass. *J. Non. Cryst. Solids* **2017**. https://doi.org/10.1016/j.jnoncrysol.2016.11.026.

(15) Shi, Y.; Ye, S.; Yu, J.; Liao, H.; Liu, J.; Wang, D. Simultaneous Energy Transfer from Molecular-like Silver Nanoclusters to Sm 3+ /Ln 3+ (Ln = Eu or Tb) in Glass under UV Excitation . *Opt. Express* **2019**. https://doi.org/10.1364/oe.380860.
(16) Malta, O. L.; Santa-Cruz, P. A.; De Sá, G. F.; Auzel, F. Fluorescence Enhancement Induced by the Presence of Small Silver Particles in Eu3+ Doped Materials. *J. Lumin.* **1985**. https://doi.org/10.1016/0022-2313(85)90003-1.
(17) Liao, H.; Ye, S.; Shen, R.; Li, X.; Wang, D. Effective Formation of Ag Nanoclusters and Efficient Energy Transfer to Yb3+ Ions in Borosilicate Glasses for Photovoltaic Application. *Mater. Res. Bull.* **2019**. https://doi.org/10.1016/j.materresbull.2018.10.042.
(18) Lin, H.; Chen, D.; Yu, Y.; Zhang, R.; Wang, Y. Molecular-like Ag Clusters Sensitized near-Infrared down-Conversion Luminescence in Oxyfluoride Glasses for Broadband Spectral Modification. *Appl. Phys. Lett.* **2013**. https://doi.org/10.1063/1.4819951.
(19) Shi, Y.; Ye, S.; Liao, H.; Liu, J.; Wang, D. Formation of Luminescent Silver-Clusters and Efficient Energy Transfer to Eu3+ in Faujasite NaX Zeolite. *J. Solid State Chem.* **2020**. https://doi.org/10.1016/j.jssc.2020.121227.
(20) Zhao, J.; Yang, Z.; Yu, C.; Qiu, J.; Song, Z. Preparation of Ultra-Small Molecule-like Ag Nano-Clusters in Silicate Glass Based on Ion-Exchange Process: Energy Transfer Investigation from Molecule-like Ag Nano-Clusters to Eu3+ Ions. *Chem. Eng. J.* **2018**. https://doi.org/10.1016/j.cej.2018.02.028.
(21) Ghafoor, M.; Sgibnev, Y.; Nikonorov, N.; Marasanov, D. Energy Transfer between Silver Clusters and Europium Eu^{3+} Ions in Photo-Thermo-Refractive Glasses; 2017. https://doi.org/10.1117/12.2271688.
(22) Vijayakumar, R.; Marimuthu, K. Luminescence Studies on Ag Nanoparticles Embedded Eu3+doped Boro-Phosphate Glasses. *J. Alloys Compd.* **2016**. https://doi.org/10.1016/j.jallcom.2016.01.049.
(23) Wei, R.; Li, J.; Gao, J.; Guo, H. Enhancement of Eu^{3+} Luminescence by Ag Species (Ag NPs, ML-Ag, Ag^{+}) in Oxyfluoride Glasses. *J. Am. Ceram. Soc.* **2012**. https://doi.org/10.1111/j.1551-2916.2012.05459.x.
(24) Guo, H.; Wang, X.; Chen, J.; Li, F. Ultraviolet Light Induced White Light Emission in Ag and Eu^3+ Co-Doped Oxyfluoride Glasses. *Opt. Express* **2010**. https://doi.org/10.1364/oe.18.018900.
(25) Jiao, Q.; Wang, X.; Qiu, J.; Zhou, D. Effect of Silver Ions and Clusters on the Luminescence Properties of Eu-Doped Borate Glasses. *Mater. Res. Bull.* **2015**. https://doi.org/10.1016/j.materresbull.2015.08.012.
(26) Maurel, C.; Cardinal, T.; Bellec, M.; Canioni, L.; Bousquet, B.; Treguer, M.; Videau, J. J.; Choi, J.; Richardson, M. Luminescence Properties of Silver Zinc Phosphate Glasses Following Different Irradiations. *J. Lumin.* **2009**, *129* (12), 1514–1518. https://doi.org/10.1016/j.jlumin.2008.12.023.
(27) Velázquez, J. J.; Tikhomirov, V. K.; Chibotaru, L. F.; Cuong, N. T.; Kuznetsov, A. S.; Rodríguez, V. D.; Nguyen, M. T.; Moshchalkov, V. V. Energy Level Diagram and Kinetics of Luminescence of Ag Nanoclusters Dispersed in a Glass Host. *Opt. Express* **2012**. https://doi.org/10.1364/oe.20.013582
(28) I. Medintz and N. Hildebrandt, *FRET – Förster Resonance Energy Transfer*, Wiley-VCH Verlag GmbH & Co. KGaA, Weinheim, **2014**.
(29) Marasanov, D. V.; Mironov, L. Yu.; Sgibnev, Y. M.; Kolesnikov I. E. and Nikonorov, N. V.; *Luminescence and energy transfer mechanisms in photo-thermo-refractive glasses co-doped*

with silver molecular clusters and Eu^{3+}, Phys. Chem. Chem. Phys., **22**, 23342-23350 (**2020**). https://doi.org/10.1039/D0CP02786C